# Methylene Blue Adsorption Mechanism onto Palm Kernel Shell-derived Activated Carbon: From Particle Diffusion to Site Adsorption

Khairul Anwar Mohamad Said,[a,b] Mohamed Afizal Mohamed Amin,[a,b] Ibrahim Yakub,[a] Md Rezaur Rahman,[a,b,*] Ahmad Beng Hong Kueh,[b,c] Sinin Hamdan,[d] and Mohammed M. Rahman [e]

The mechanism of methylene blue adsorption was investigated for palm kernel shell-derived activated carbon from the bulk solution to active sites. For different initial dye concentrations, 100 ppm methylene blue led to approximately 10 mg/g adsorption capacity while experiencing a decreasing trend at lower initial dye concentrations as follows: 50 ppm (approximately 5 mg/g) > 20 ppm (approximately 2 mg/g) > 5 ppm (approximately 0.5 mg/g). Based on the Boyd external diffusion model, the mechanism of methylene blue adsorption started with its diffusion from the bulk solution *via* the bounding film encapsulating the activated carbon. The adsorbed species occupied more than one class of active site with an adsorption rate of 0.54 mg/g.min, while the adsorption capacity accounted for 14.7 mg/g. The information about methylene blue offers useful insights into describing the steps of dye adsorption onto palm kernel shell-activated carbon.

*DOI: 10.15376/biores.18.3.5120-5132*

*Keywords: Palm kernel shell; Adsorption; Methylene blue; Kinetic; Isotherm; Activated carbon*

*Contact information: a: Department of Chemical Engineering and Energy Sustainability, Faculty of Engineering, Universiti Malaysia Sarawak, 94300 Kota Samarahan, Sarawak, Malaysia; b: UNIMAS Water Centre (UWC), Faculty of Engineering, Universiti Malaysia Sarawak, 94300 Kota Samarahan, Sarawak, Malaysia; c: Department of Civil Engineering, Faculty of Engineering, Universiti Malaysia Sarawak, 94300 Kota Samarahan, Sarawak, Malaysia; d: Department of Mechanical Engineering, Faculty of Engineering, Universiti Malaysia Sarawak, 94300 Kota Samarahan, Sarawak, Malaysia; e: Department of Chemistry, King Abdulaziz University, Jeddah 21589, Saudi Arabia & Center of Excellence for Advanced Materials Research (CEAMR), King Abdulaziz University, Jeddah 21589, Saudi Arabia; *Corresponding author: rmrezaur@unimas.my*

## INTRODUCTION

Rapid industrialization worldwide has led to severe water scarcity, primarily because of contamination by many pollutants. Organic dye is one type of contaminant that is widely used in many industries, such as textiles, paper production, and plastics. Organic dye released as industrial waste with high toxicity would cause serious health effects on living things and ultimately damage the environment. Given the dye's toxicity and color, researchers have investigated various methods for dye removal from wastewater, such as membrane separation, adsorption, chemical oxidation, and photocatalysis. Although most technology could remove dye sufficiently below the limit set by the governing body, adsorption has several advantages compared to other technologies, such as low-cost operation and capital, the ability to operate despite the presence of many toxic substances,

and simple operation. Moreover, as a result of research regarding adsorption, many materials have been synthesized primarily for dye adsorption.

For instance, Melendez-Ortiz *et al.* (2014) synthesized MCM-41 and MCM-48 with mesocellular silica foam (MCF) for dye removal applications. Their findings showed that dye adsorption performance was directly proportional to the increase in pH, adsorbent dosage, and contact time while increasing the temperature negatively impacted the adsorption performance. In addition to materials based on silica, various metal-organic frameworks (MOF) have been synthesized for dye adsorption applications. The MOF's unique surface and framework are the main factors that distinguish their dye adsorption. Cai *et al.* (2020) developed MXene composite materials for dye removal, which positively improve the dye adsorption capacity. Another area of adsorption worth mentioning is the activated carbon derived from biomaterials such as wood, leaves, and fruit stone (Cai *et al.* 2020). Ebadollahzadeh and Zabihi (2020) investigated the possibility of activated carbon derived from peach stone and wood to remove methylene blue and Pb(II). Their findings showed that the adsorption of lead ions was low compared to methylene blue. Lead had a maximum adsorption capacity of 61.8 mg/g, while the adsorption of methylene blue soared up to 438 mg/g (Ebadollahzadeh and Zabihi 2020). This was attributed to adsorbent properties and the type of adsorbate molecules. Cheng *et al.* (2021) synthesized biochar from sludge and liriodendron leaves and loaded the biochar with iron to improve its performance because of the presence of Cr(VI) in the mixture of methyl orange. It was found that the presence of heavy metal reduced the methyl orange adsorption (Cheng *et al.* 2021). Despite the increment in methyl orange concentration, the removal performance kept decreasing until the methyl orange concentration surpassed 0.6 mmol/L, thereafter showing positive results with increased methyl orange adsorption. Meanwhile, Yu *et al.* (2018) synthesized porous activated carbon from banana peels. Initially, the dye adsorption capacity was lower than Co(II) adsorption in the mixture of both pollutants and even lower compared to dye-only solution and *vice versa* for Co(II) adsorption in a single component solution (Yu *et al.* 2018). However, increasing the amount of dye in the mixture showed a notable increase in dye adsorption capacity compared to the Co(II) adsorption. Another plant-based activated carbon as derived from the cacti plant *Opuntia ficus-indica* was investigated by Choudhary *et al.* (2020). The activated carbon was used to perform adsorption on Cu(II), Ni(II), and malachite green, with the result that the adsorption capacity was found to be directly proportional to the activation intensity (Choudhary *et al.* 2020). While the adsorption capacity of malachite green was the lowest for biochar, the carbon activated by sodium hydroxide (NaOH), especially at a 1:2 ratio of biochar to NaOH exhibited the highest removal. Meanwhile, the Cu(II) adsorption capacity depended on the activation method, while the type of adsorbent being utilized drove the Ni(II) adsorption capacity. For a ternary solution consisting of all pollutants, the presence of both heavy metals affected malachite green adsorption capacity compared to a single component solution.

Despite all the studies conducted on the activated carbon, the understanding of the mechanism of adsorbate-adsorbent interaction is still lacking, whereby most studies have been limited to fitting the adsorption data to common isotherm and kinetic models such as Langmuir, Freundlich, pseudo-first-order, and pseudo-second-order. Therefore, this study explores the mechanism of adsorption from the transfer of adsorbate from the bulk solution to its adsorption on the active site, including the phenomena that occur on the active site.

## EXPERIMENTAL

### Materials

Activated carbon was supplied by the local vendor at Kota Samarahan, Malaysia. It was produced from palm oil kernel shells. The manufacturer employed pyrolysis during the production of carbon, followed by steam activation. The activated carbon was dried overnight at 70 °C before the adsorption test. The dried activated carbon was pulverized with a mortar prior to the adsorption test. All batch tests were regulated to pH 7 with HCl or NaOH solution, which was performed at room temperature (25 to 28 °C). The activated carbon was characterized by Fourier transform infrared spectroscopy (IRAFFINITY-1, Shimadzu, Kyoto, Japan) from 4000 to 400 $cm^{-1}$ to identify the functional group and scanning electron microscopy (TM4000, Hitachi, Tokyo, Japan) to study the morphological properties.

The adsorption test was conducted with 5, 20, 50, and 100 ppm initial concentrations ($C_0$) of methylene blue. The dye volume was fixed at 500 mL during the batch adsorption experiment, while contact time and initial concentration were varied. Meanwhile, the mass of activated carbon was 1.0 g for all tests. The residual dye concentration was analyzed by ultraviolet-visible (UV-vis) spectrophotometer (UV-1800; Shimadzu, Kyoto, Japan) at 665 nm.

The adsorption capacity of activated carbon was calculated using Eq. 1 (Mohamad Said *et al.* 2022),

$$q_e = \frac{(C_0 - C_e) \times V}{W} \quad (1)$$

where $q_e$ refers to dye adsorption at equilibrium (mg/g), $C_o$ and $C_e$ are the initial and dye concentrations at equilibrium (mg/L), respectively, $V$ is the volume of dye solution (L), and $m$ is the activated carbon mass fixed at 1 g.

The adsorption data were fitted to the kinetic model classified as adsorption reaction (pseudo-first-order, pseudo-second-order, Ritchie, Ritchie-second-order, and mixed-order models) and diffusion models (Boyd equation and Weber and Morris) to understand the dye adsorption mechanism. Meanwhile, the mode of dye adsorption was investigated by fitting the adsorption data to isotherm models such as Langmuir and Freundlich. The model validity was determined by the coefficient of determination ($R^2$), chi-square ($\chi^2$), and the sum of squares (SSE).

## RESULTS AND DISCUSSION

### Particle Morphology

The pulverized activated carbon in fine powder form is presented in Fig. 1. Figure 2 illustrates the activated carbon surface and close-up pore. Figure 2(a) shows that the surface was smooth with apparent pores scattered across it. The pore sizes were varied and can be identified by the blackened dots. Meanwhile, the pore size at the close-up range (Fig. 2(b)) shows that the surface around the pore was coarser than in Fig. 2(a). In Fig. 2(b), the pores located in the middle were around 5 microns.

**Fig. 1.** Pulverized activated carbon

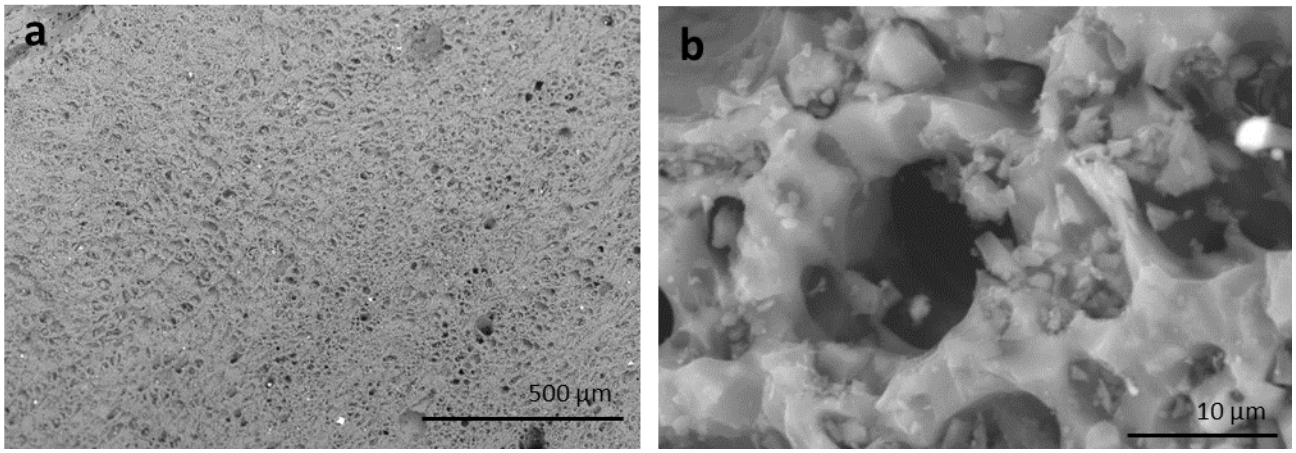


**Fig. 2.** SEM images for (a) activated carbon surface and (b) activated carbon pore

Table 1 summarizes the physical properties of the activated carbon. The BET analysis indicates that the activated carbon had a specific surface area of 500 $m^2$/g.

**Table 1.** Physical Properties of Activated Carbon

| | |
|---|---|
| BET Specific Surface Area | 500 $m^2$ /g |
| T plot Micropore Volume | $2.53 \times 10^{-1}$ $cm^3$ /g |
| Cumulative Adsorption Surface Area (BJH Method) | 54.2 $m^2$ /g |
| Pore Radius | $1.011 \times 10^{-7}$cm |

In comparison, Lee *et al.* (2021) employed coconut shells (CS) and palm kernel shells (PKS) in the pretreatment stages to evaluate their influence on activated carbon production. The CS and PKS had specific surface areas of 0.84 and 0.79 $m^2$/g, respectively (Lee *et al.* 2021). Once pretreated, even soaking CS and PKS in hot water at 80 °C could increase the specific surface areas to 8.37 and 6.45 $m^2$/g, respectively. Another pretreatment method was to soak the materials in sodium hydroxide and phosphoric acid, which revealed that soaking in phosphoric acid led to the highest specific surface areas of 11.62 and 8.76 $m^2$/g for CS and PKS, respectively. Meanwhile, soaking the materials in

alkaline solution or sodium hydroxide reduced the specific surface area below the pretreatment with water at 6.34 (CS) and 4.68 (PKS) $m^2/g$. Hence, the specific surface area of the activated carbon in this study was many folds higher than the pristine material, which is eventually made into activated carbon, such as coconut shells and palm kernel shells.

The Barrett-Joyner-Halenda (BJH) cumulative adsorption surface area for the activated carbon was observed as 54 $m^2/g$ with a micropore volume of $2.5 \times 10^{-1}$ $cm^3$ /g. The micropore volume of this activated carbon can be considered higher than average. Zainal *et al.* (2018) synthesized PKS by carbonizing the material at 500 °C for 3 h and then steaming the carbonized PKS for another 3 h at 700 °C. Despite the high-temperature treatment, the micropore volume of PKS was only 0.09 $cm^3/g$ (Zainal *et al.* 2018). It was 64% smaller than the present activated carbon even though it originated from similar materials. The smaller micropore volume of PKS synthesized by Zainal *et al.* (2018) might be a result of the short carbonization step duration and lack of a chemical activation agent. Another way to increase the surface area of activated carbon is by increasing the activation temperature, which leads to pore enlargement while creating new pores.

However, an activation temperature above optimal may reduce the activated carbon yield because of the release of volatile compounds. Table 2 lists existing literature of synthesizing activated carbon from biomass. From the list, only two biomass specimens achieved a surface area below the surface area of palm kernel shell in this study, date palm tree and yellow mombin fruit stones. Celery, a vegetable, yielded the highest surface area compared to any other biomass and was activated by carbonization without an activating agent (Khosrowshahi *et al.* 2022). Based on the relationship between activation temperature and activating agent to the surface area, it can be concluded that a combination of high temperature with an activating agent can lead to higher surface area in most cases despite the high surface area of the initial celery. For celery-activated carbon, the closed-loop activation chamber may contribute to its high surface area with no assistance from an activating agent. For the closed-loop chamber, the gaseous by-product from pyrolysis will be circulated inside the chamber, while air will be supplied inside the chamber *via* a pump. Thus, it is possible to self-activate the biomass using a one-step process.

**Table 2.** Comparison of Activated Carbon from Various Forms of Biomass

| Biomass | Activating Agent | Activation Temperature (°C) | Surface Area ($m^2/g$) | References |
|---|---|---|---|---|
| Date palm tree | $CO^2$ | 576 | 385 | Shoaib and Al-Swaidan (2015) |
| Yellow mombin fruit stones | KOH | 222 | 12.5 | (Brito *et al.* 2017) |
| Pine dust | High-pressure steam | 900 | 962 | (Yang and Cannon 2022) |
| Celery | Synthetic gas | 700 | 1126 | (Khosrowshahi *et al.* 2022) |
| Oil palm kernel shell | Steam | 250 | 678 | (Nahrul Hayawin *et al.* 2020) |
| Coconut shell | NaOH | 700 | 850 | (Trisunaryanti *et al.* 2022) |
| Pam kernel shell | N/A | N/A | 500 | This study |

## Effects of Initial Dye Concentration

Figure 3 illustrates the activated carbon's performance in adsorbing methylene blue at different initial concentrations. At low initial concentrations (5 and 20 ppm), the adsorption rate began to slow when reaching the first 20 min. For 5 ppm initial concentration, the adsorption capacity reached equilibrium ($q_e$) at 0.41 mg/g after 20 min of adsorption. Meanwhile, for the 20-ppm initial concentration, the adsorption equilibrium was recorded at 2 mg/g, which started in the 60$^{th}$ min of adsorption.

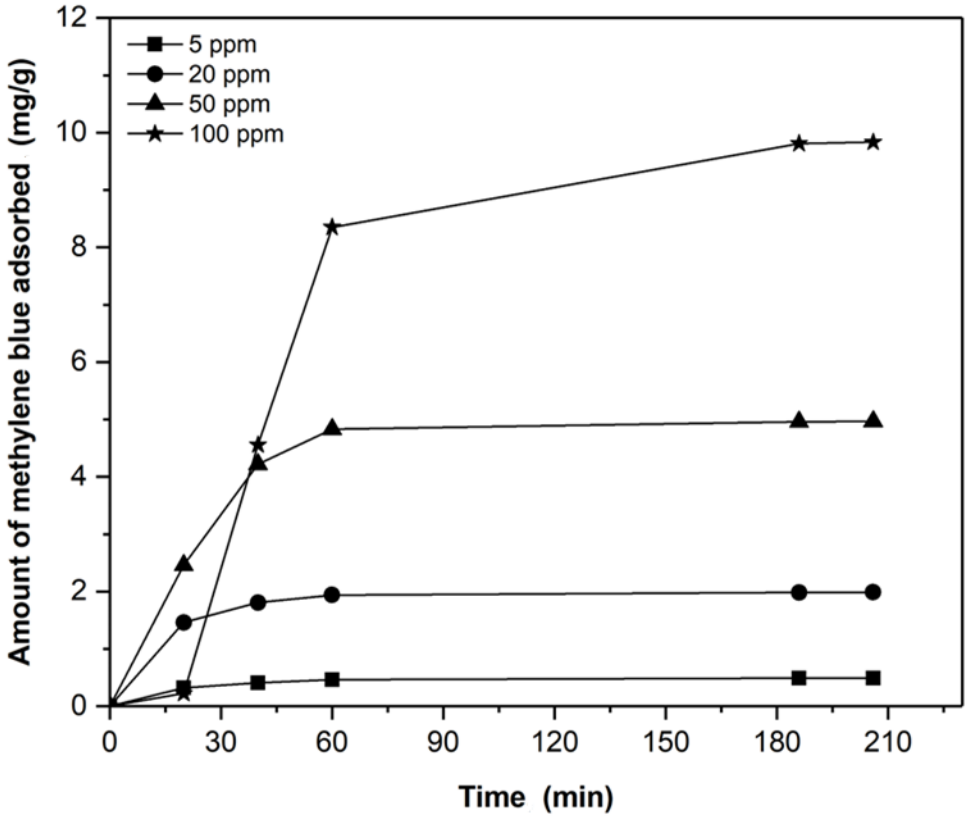


**Fig. 3.** Adsorption amount of methylene blue at varied initial concentrations

## Mechanism of Adsorption Based on Isotherm and Kinetic Models

Table 3 summarizes the kinetic models that fit the experimental adsorption data. The pseudo-first-order model, which also is known as the Lagergren equation, is the first ever model to describe the adsorption interaction between solid and liquid interface. Lagergren proposed the idea when explaining the adsorption of oxalic and malonic acid on a carbon material. However, the theoretical derivation of the pseudo-first-order was only available 100 years after its proposal. This derivation was contributed by Azizian in 2004, based on the theory of activated adsorption/desorption (TAAD) (Azizian 2004). For a long adsorption time, the Lagergren equation, in which the adsorption reaches a position that is not far from the equilibrium state, with the pseudo-first-order kinetic feature will become closely similar to the expression of the diffusional model (Azizian and Eris 2021).

Based on the statistical evaluation with $R^2$, the sum of squares, and chi-square, the adsorption rate data showed a favorable fit with the pseudo-first-order model. In the case of the Weber and Morris model, the model fitting is poor based on the value of $R^2$, chi-square, and SSE. According to Wang and Guo (2019), the plot of Weber and Morris model

fitting should exhibit a straight line that start from the origin to indicate an intraparticle diffusion mechanism (Guo and Wang 2019). Thus, it can be concluded here that the adsorption for internal or intraparticle diffusion was controlled by multiple phenomena. Therefore, the rate of methylene blue adsorption was judged to be consistent with a diffusion mechanism, which may involve pore volume diffusion, adsorbent exterior diffusion, or a combination of both.

Hence, the postulation regarding external diffusion of dye onto activated carbon has also been proposed by Boyd (1947). In the proposal, it is noted that external diffusion is the main rate-controlling step during the initial moments of an adsorption process, or maybe during an extensive period in the absence of stirring (Boyd *et al.* 1947). The Boyd equation was derived based on Fick's second law, which describes the adsorption and ion exchange that takes place between aqueous solution and zeolite. Based on the Boyd adsorption model, activated carbon's shape can be assumed as spherical and has a similar size, which also influences its nomenclature in the literature. The Boyd equation is also known as the homogenous particle diffusion model. Wang and Guo (2020b) classified the Boyd adsorption model under the external diffusion model based on the adsorption phenomenon (Wang and Guo 2020). The original idea by Boyd (1947) states that diffusion at the boundary of the liquid film can be divided into five steps. All of the steps proposed by Boyd are based on the following chemical reaction $A^+ + BR \leftrightarrow AR + B^+$, in which $A^+$ and $B^+$ represent the exchanging monovalent cations while R is the fixed-in-place anionic fraction of the adsorbent. From the perspective of methylene blue adsorption onto activated carbon, $A^+$ and $B^+$ represent the diffusions of dye pigment from the bulk solution onto the activated carbon and diffusion out of the adsorption site to the bulk solution. The nomenclatures A and B are to differentiate the direction of dye pigment either adsorption or desorption from the site, although they represent similar material. For external diffusion that occurs at the bounding liquid film, from all the five steps of diffusion proposed by Boyd, the two steps that preferably will be eliminated are the first and the last step. The first step occurs when the dye pigment enters the boundary film from the bulk solution, while the last step is the diffusion of desorbed dye pigment into the bulk solution. Therefore, the adsorption experiment is conducted with vigorous mixing to minimize these two steps' effects. For boundary film diffusion, the shape of the adsorbent is assumed to be spherical with a radius of $r_o$ and it is surrounded by a liquid film with a radius of $r_o'$. Hence, the thickness of the boundary film can be represented as $\Delta r = r_o' - r_o$. At equilibrium, by minimizing the occurrence of bulk to adsorption site adsorption and desorption (steps 1 and 5), it can be assumed that $r = r_o$. Hence, it can be inferred that the total quantity of adsorbate on one adsorbent, $Q$, is directly proportional to $C^s/\kappa$, in which the distribution coefficient, $\kappa$, is independent of concentration. Thus, at equilibrium, the concentration in solid, $C^s$, can be assumed as $Q/r_o$, considering that the denominator is mostly constant except for $r_o$. At equilibrium, the concentration of solid and liquid can be related by the distribution coefficient, $\kappa$:

$$C^s / \kappa = \frac{Q}{4/3(\pi r_o^3 \kappa)} \quad (2)$$

The simplified form of Eq. 2 can be written as:

$$C^s = \frac{Q}{4/3(\pi r_o^3)} \quad (3)$$

Assuming $r_o$ is constant, it can be concluded that:

$$C^s \propto \frac{Q}{4/3(\pi)} \quad (4)$$

Therefore, based on the diffusion mechanism by Boyd (1947), specifically the diffusion through film encapsulating adsorbent, it can be assumed that diffusion of methylene blue from the bulk solution would be controlled by diffusion through the bounding film.

For the adsorption at the active sites, the Ritchie equation assumes that the adsorption is driven by the adsorption that occurs at active sites. Hence, the Ritchie equation can estimate the number of active sites, *n*, occupied by a single adsorbate ion or molecule. Ritchie equation could be transformed to second order when the value of *n* is 2. Based on Table 3, from Ritchie equation, one dye molecule can occupy 1.21 active sites on activated carbon. Assuming the dye molecule did not uniformly occupy $n = 1.21$ and a dye molecule could occupy two active sites based on Ritchie second-order (refer to Table 3), the model validity is favorable. Hence, it is inferred that the methylene blue adsorption onto the active site could occupy more than one active site, thus reducing the relative efficiencies of the activated carbon.

To summarize, the external diffusion from bulk liquid has been proposed by the Boyd equation, while the adsorption that occurs on the active site has been discussed using the Ritchie equation, including its second-order form.

**Table 3.** Kinetic Model of Methylene Blue Adsorption onto Activated Carbon

| | | | | | | |
|---|---|---|---|---|---|---|
| **Pseudo-first-order** | $k_1$ | $q_e$ | $R^2$ | **Chi-square** | **SSE** | |
| | 0.051 | 0.487 | 0.99 | 0.001 | 0.0001 | |
| | | | | | | |
| **Pseudo-second-order** | $k_2$ | $q_e$ | $R^2$ | **Chi-square** | **SSE** | |
| | 0.16 | 0.527087 | 0.99 | 0.00147 | 0.00061 | |
| | | | | | | |
| **Ritchie** | **Alpha** | ***n*** | $q_e$ | $R^2$ | **chi-square** | **SSE** |
| | 0.058 | 1.20 | 0.49 | 0.99 | 0.00016 | 7.06E-05 |
| | | | | | | |
| **Ritchie Second Order** | **Alpha** | $q_e$ | $R^2$ | **Chi-square** | **SSE** | |
| | 0.12 | 0.49 | 0.98 | 0.0057 | 0.0023 | |
| | | | | | | |
| **Boyd** | **R** | $q_e$ | $R^2$ | **Chi-square** | **SSE** | |
| | 0.0496 | 0.49 | 0.99 | 0.00083 | 0.0003 | |
| | | | | | | |
| **Weber and Morris** | $K_{w\&m}$ | $R^2$ | **Chi-square** | **SSE** | | |
| | 0.042 | 0.78 | 0.27 | 0.076 | | |

Table 4 lists the isotherm models associated with methylene blue adsorption onto activated carbon. Based on the model fitted, the coefficient of determination ($R^2$) shows that Langmuir offer an $R^2$ closer to 1.

When applying the Langmuir isotherm model, it is assumed that each adsorption site is equal, and that the filling of an adsorption site does not affect adsorption on adjacent sites (Langmuir 1918). Based on the Langmuir model fitting, the maximum adsorption capacity that the activated carbon could exhibit is 14.7 mg/g, meaning that for every 1 g of activated carbon, it can hold around 14 mg of methylene blue. Therefore, if the initial dye concentration is capped at 500 mg/L (ppm), and it would require 35 g of activated carbon to adsorb all of the dye. In addition to the determination of maximum adsorption capacity, the separation factor ($R_L$) can be identified by the following Eq. 5,

$$R_L = \frac{1}{1 + K_L C_o} \quad (5)$$

where the initial dye concentration ($C_o$) is 100 ppm and the calculated $R_L$ is 0.009, which is lower than 1, thus signifying the adsorption to be favorable.

**Table 4.** Isotherm Model of Methylene Blue Adsorption onto Activated Carbon

| | KL | $q_{max}$ | $R^2$ | Chi-square | SSE | | |
|---|---|---|---|---|---|---|---|
| Langmuir | 1.16 | 14.70 | 0.97 | 0.691 | 1.20 | | |
| | KF | n | $R^2$ | Chi-square | SSE | | |
| Freundlich | 7.048 | 1.64 | 0.94 | 1.16 | 2.68 | | |

Figure 4 presents the FTIR spectra for the membrane before and after the methylene blue removal.

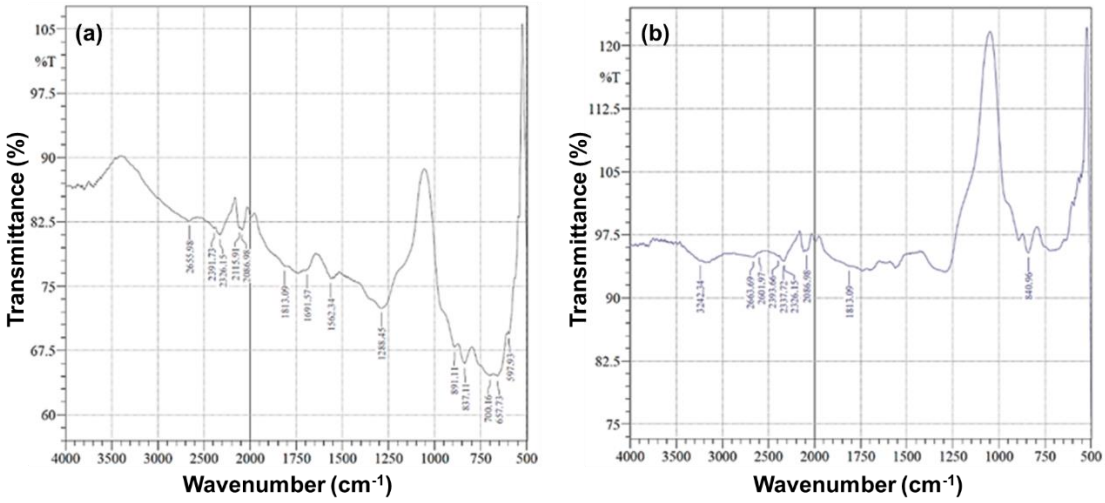


**Fig. 4.** FTIR spectra (a) before and (b) after adsorption

Tables 5 and 6 summarize the peak wavenumbers from the FTIR spectrum of activated carbon before and after the adsorption. Although the spectrum for each activated carbon looks alike, the shift to higher intensity is noticeable for used activated carbon. For instance, at 1813 $cm^{-1}$, which accounts for the C-H bending of an aromatic compound, the intensity of the peak before adsorption was 78% and it increased to 93% after methylene blue adsorption. The chemical structure of methylene blue shows that it is comprised of

three benzene rings, thus contributing to the increase in the intensity of the FTIR peak at 1813 $cm^{-1}$. Hence, it can be inferred that activated carbon can adsorb methylene blue. In general, the FTIR spectra were recorded from 4000 to 500 $cm^{-1}$, in which after the adsorption, a new peak appeared at 3500 to 3000 $cm^{-1}$, accounting for O-H stretching. The presence of O-H at this wavenumber normally indicates the presence of water molecules inside the activated carbon pores (Wibawa *et al.* 2020).

**Table 5.** FTIR Spectra of the Activated Carbon before Adsorption

| No. | Peak Wavenumber ($cm^{-1}$) | Appearance | Functional Group | Compound Class |
|---|---|---|---|---|
| 1 | 837.11 | Strong | C-Cl stretching | Halo compound |
| 2 | 891.11 | Strong | C-H bending | 1,2,4-trisubstituted |
| 3 | 1288.45 | Strong | C-O stretching | Aromatic ester |
| 4 | 1691.57 | Strong | C=O stretching | Conjugated aldehyde |
| 5 | 1813.09 | Weak | C-H bending | Aromatic compound |
| 6 | 2086.98 | Strong | N=C=S bending | Isothiocyanate |
| 7 | 2115.91 | Weak | C=C stretching | Alkyne |

**Table 6.** FTIR Spectra of the Activated Carbon after Adsorption

| No. | Peak Wavenumber ($cm^{-1}$) | Appearance | Functional Group | Compound Class |
|---|---|---|---|---|
| 1 | 840.96 | Strong | C-Cl stretching | Halo compound |
| 2 | 1813.09 | Weak | C-H bending | Aromatic compound |
| 3 | 2086.98 | Strong | N=C=S bending | Isothiocyanate |
| 4 | 2601.97 | Strong, Broad | O-H stretching | Intramolecular bonded alcohol |
| 5 | 2663.69 | Strong, Broad | O-H stretching | Intramolecular bonded alcohol |
| 6 | 3242.34 | Strong, Broad | O-H stretching | Intramolecular bonded alcohol |

## CONCLUSIONS

1. The mechanism of methylene blue adsorption onto activated carbon has been considered based on several adsorption kinetic and isotherm models. The kinetic adsorption models that best fit the adsorption phenomenon of dye onto activated palm kernel shells are Ritchie and Boyd models. Meanwhile, the isotherm adsorption model are based on Langmuir model.
2. The SEM micrograph shows that the surface was smooth with apparent pores scattered across it. BET analysis indicates that the activated carbon had a specific surface area of 500 $m^2/g$, with the BJH cumulative adsorption surface area for the activated carbon recorded at 54 $m^2/g$ with a micropore volume of $2.5 \times 10^{-1}$ $cm^3$ /g, which is higher than average biomass-based activated carbon.
3. The adsorption isotherm data were in good agreement with the Langmuir model, which assumes adsorption at energetically equal sites that do not affect each other.

## ACKNOWLEDGMENTS

The authors would like to extend their appreciation to the Universiti Malaysia Sarawak (UNIMAS), for managing the research activity. We also would like to express gratitude to the Osaka Gas Foundation of International Cultural Exchange (OGFICE) (INT/F02/OSAKA-IG/85662/2023) for funding.

## REFERENCES CITED

Azizian, S. (2004). "Kinetic models of sorption: A theoretical analysis," *Journal of Colloid and Interface Science* 276(1), 47-52. DOI: 10.1016/j.jcis.2004.03.048

Azizian, S., and Eris, S. (2021). "Adsorption isotherms and kinetics," in: *Adsorption: Fundamental Processes and Applications*, Elsevier Ltd., Andover, MA, USA, pp. 445-509. DOI: 10.1016/B978-0-12-818805-7.00011-4

Boyd, G. E., Adamson, A. W., and Myers, L. S. (1947). "The exchange adsorption of ions from aqueous solutions by organic zeolites. II. Kinetics 1," *Journal of the American Chemical Society* 69(11), 2836-2848. DOI: 10.1021/ja01203a066

Brito, M. J. P., Veloso, C. M., Bonomo, R. C. F., Fontan, R. da C. I., Santos, L. S., and Monteiro, K. A. (2017). "Activated carbons preparation from yellow mombin fruit stones for lipase immobilization," *Fuel Processing Technology* 156, 421-428. DOI: 10.1016/j.fuproc.2016.10.003

Cai, W., Cheng, X., Chen, X., Li, J., and Pei, J. (2020). "Poly(vinyl alcohol)-modified membranes by Ti3C2Tx for ethanol dehydration *via* pervaporation," *ACS Omega* 5(12), 6277-6287. DOI: 10.1021/acsomega.9b03388

Cheng, H., Liu, Y., and Li, X. (2021). "Adsorption performance and mechanism of iron-loaded biochar to methyl orange in the presence of $Cr^{6+}$ from dye wastewater," *Journal of Hazardous Materials* 415, article ID 125749. DOI: 10.1016/j.jhazmat.2021.125749

Choudhary, M., Kumar, R., and Neogi, S. (2020). "Activated biochar derived from *Opuntia ficus-indica* for the efficient adsorption of malachite green dye, $Cu^{+2}$ and $Ni^{+2}$ from water," *Journal of Hazardous Materials* 392, article ID 122441. DOI: 10.1016/j.jhazmat.2020.122441

Ebadollahzadeh, H., and Zabihi, M. (2020). "Competitive adsorption of methylene blue and Pb (II) ions on the nano-magnetic activated carbon and alumina," *Materials Chemistry and Physics* 248, article ID 122893. DOI: 10.1016/j.matchemphys.2020.122893

Guo, X., and Wang, J. (2019). "A general kinetic model for adsorption: Theoretical analysis and modeling," *Journal of Molecular Liquids* 288, article ID 111100. DOI: 10.1016/j.molliq.2019.111100

Khosrowshahi, M. S., Mashhadimoslem, H., Emrooz, H. B. M., Ghaemi, A., and Hosseini, M. S. (2022). "Green self-activating synthesis system for porous carbons: Celery biomass wastes as a typical case for $CO_2$ uptake with kinetic, equilibrium and thermodynamic studies," *Diamond and Related Materials* 127, article ID 109204. DOI: 10.1016/j.diamond.2022.109204

Langmuir, I. (1918). "The adsorption of gases on plane surfaces of glass, mica and platinum," *Journal of the American Chemical Society* 40(9), 1361-1403. DOI: 10.1021/ja02242a004

Lee, C. L., Chin, K. L., H'ng, P. S., Rashid, U., Maminski, M., and Khoo, P. S. (2021). "Effect of pretreatment conditions on the chemical–structural characteristics of coconut and palm kernel shell: A potentially valuable precursor for eco-efficient activated carbon production," *Environmental Technology and Innovation* 21, article ID 101309. DOI: 10.1016/j.eti.2020.101309

Meléndez-Ortiz, H. I., Perera-Mercado, Y., Mercado-Silva, J. A., Olivares-Maldonado, Y., Castruita, G., and García-Cerda, L. A. (2014). "Functionalization with amine-containing organosilane of mesoporous silica MCM-41 and MCM-48 obtained at room temperature," *Ceramics International* 40(7, Part A), 9701-9707. DOI: 10.1016/j.ceramint.2014.02.051

Mohamad Said, K. A., Ismail, A. F., Zulhairun, A. K., Abdullah, M. S., Azali, M. A., and Zainal Abidin, M. N. (2022). "Magnetic induced asymmetric membrane: Effect of magnetic pattern to phenol removal by adsorption," *Materials Chemistry and Physics* 278(August 2021), article ID 125692. DOI: 10.1016/j.matchemphys.2021.125692

Nahrul Hayawin, Z., Ibrahim, M. F., Nor Faizah, J., Ropandi, M., Astimar, A. A., Noorshamsiana, A. W., and Abd-Aziz, S. (2020). "Palm oil mill final discharge treatment by a continuous adsorption system using oil palm kernel shell activated carbon produced from two-in-one carbonization activation reactor system," *Journal of Water Process Engineering* 36, article ID 101262. DOI: 10.1016/j.jwpe.2020.101262

Shoaib, M., and Al-Swaidan, H. M. (2015). "Optimization and characterization of sliced activated carbon prepared from date palm tree fronds by physical activation," *Biomass and Bioenergy* 73, 124-134. DOI: 10.1016/j.biombioe.2014.12.016

Trisunaryanti, W., Wijaya, K., Triyono, T., Wahyuningtyas, N., Utami, S. P., and Larasati, S. (2022). "Characteristics of coconut shell-based activated carbon as Ni and Pt catalyst supports for hydrotreating *Calophyllum inophyllum* oil into hydrocarbon-based biofuel," *Journal of Environmental Chemical Engineering* 10(5), article ID 108209. DOI: 10.1016/j.jece.2022.108209

Wang, J., and Guo, X. (2020a). "Adsorption kinetic models: Physical meanings, applications, and solving methods," *Journal of Hazardous Materials* 390(November 2019), article ID 122156. DOI: 10.1016/j.jhazmat.2020.122156

Wang, J., and Guo, X. (2020b). "Adsorption isotherm models: Classification, physical meaning, application and solving method," *Chemosphere* 258, article ID 127279. DOI: 10.1016/j.chemosphere.2020.127279

Wibawa, P. J., Nur, M., Asy'ari, M., and Nur, H. (2020). "SEM, XRD and FTIR analyses of both ultrasonic and heat generated activated carbon black microstructures," *Heliyon* 6(3), article ID e03546. DOI: 10.1016/j.heliyon.2020.e03546

Yang, Y., and Cannon, F. S. (2022). "Biomass activated carbon derived from pine sawdust with steam bursting pretreatment; perfluorooctanoic acid and methylene blue adsorption," *Bioresource Technology* 344, article ID 126161. DOI: 10.1016/j.biortech.2021.126161

Yu, D., Wang, L., and Wu, M. (2018). "Simultaneous removal of dye and heavy metal by banana peels derived hierarchically porous carbons," *Journal of the Taiwan Institute of Chemical Engineers* 93, 543-553. DOI: 10.1016/j.jtice.2018.08.038

Zainal, N. H., Aziz, A. A., Ibrahim, M. F., Idris, J., Hassan, M. A., Bahrin, E. K., Jalani, N. F., Wafti, N. S. A., and Abd-Aziz, S. (2018). "Carbonisation-activation of oil palm kernel shell to produce activated carbon and methylene blue adsorption kinetics," *Journal of Oil Palm Research* 30(3), 495-502. DOI: 10.21894/jopr.2018.0039

Article submitted: February 15, 2023; Peer review completed: April 8, 2023; Revisions received and accepted: May 31, 2023; Published: June 8, 2023.
DOI: 10.15376/biores.18.3.5120-5132